2007

Phase stability and consolidation of glassy/ nanostructured Al85Ni9Nd4Co2 alloys

Laichang Zhang
IFW Dresden, laichang@uow.edu.au

M Calin
University of Bucharest

M Branzei
University of Bucharest

L Schultz
IFW Dresden

J Eckert
IFW Dresden

Publication Details

Zhang, L. C., Calin, M., Branzei, M., Schultz, L. Eckert, J. (2007). Phase stability and consolidation of glassy/nanostructured Al85Ni9Nd4Co2 alloys. Journal of Materials Research, 22 (5), 1145-1155.

Phase stability and consolidation of glassy/nanostructured $Al_{85}Ni_9Nd_4Co_2$ alloys

L.C. Zhang[a)]
Fachgebiet Physikalische Metallkunde, Fachbereich 11-Material- und Geowissenschaften, Technische Universität Darmstadt, D-64287 Darmstadt, Germany; and Institut für Komplexe Materialien, IFW Dresden, D-01171 Dresden, Germany

M. Calin
Fachgebiet Physikalische Metallkunde, Fachbereich 11-Material- und Geowissenschaften, Technische Universität Darmstadt, D-64287 Darmstadt, Germany; and Materials Science and Engineering Faculty, University "Politehnica" of Bucharest, R-060032 Bucharest, Romania

M. Branzei
Materials Science and Engineering Faculty, University "Politehnica" of Bucharest, R-060032 Bucharest, Romania

L. Schultz
Institut für Metallische Werkstoffe, IFW Dresden, D-01171 Dresden, Germany

J. Eckert[b)]
Fachgebiet Physikalische Metallkunde, Fachbereich 11-Material- und Geowissenschaften, Technische Universität Darmstadt, D-64287 Darmstadt, Germany; and Institut für Komplexe Materialien, IFW Dresden, D-01171 Dresden, Germany

(Received 3 June 2006; accepted 2 August 2006)

$Al_{85}Ni_9Nd_4Co_2$ metallic glass/nanostructured ribbons and powders were used as starting materials for producing bulk amorphous/nanostructured Al-based alloys. Glassy ribbons were obtained by melt spinning at wheel surface velocities ranging from 5 to 37 m/s. The amorphous ribbons exhibited a supercooled liquid region of ~20 K, a reduced glass transition temperature of ~0.47 and $\gamma \sim 0.328$. Mechanical alloying of the elemental powder mixture did not lead to amorphization. However, amorphous powders obtained by milling the glassy ribbons for 9 h exhibited a thermal stability similar to the initial ribbons. Isothermal differential scanning calorimetry measurements were used to determine the consolidation parameters of the glassy powders. Consolidation at 513 K by uniaxial hot pressing and hot extrusion indicated that the former method leads to bulk glassy samples, whereas the latter one yields nanostructured α-Al/glassy matrix composites.

I. INTRODUCTION

The development of lightweight alloys is of great importance for meeting new requirements in various fields, i.e., for transportation systems and energy consumption. In this context, aluminum- and titanium-based alloys have achieved major importance for advanced structural applications due to their high specific strength combined with good corrosion resistance.[1,2] On the other hand, bulk metallic glasses (BMGs) have potential for applications as new high-strength structural materials due to their excellent mechanical properties such as high elastic modulus and strength in comparison with their corresponding crystalline counterparts.[3,4] The achievement of BMG formation[3,4] and new types of marginal glass-forming systems such as Al-TM-RE alloys (TM = transition metal, RE = rare-earth metal)[5–9] has extended the understanding of some of the basic factors underlying glass formation. A remarkable characteristic of these aluminum-based alloy systems is that the alloys contain >85 at.% of the base component and do not have a deep eutectic, which has been a common guideline for easy glass formation.[7] The favored compositions for glass formation in Al-TM-RE alloy systems have melting temperatures higher than that of the pure aluminum.[8,9] Instead of a deep eutectic, it appears that a multicomponent combination of constituents with large atomic size differences (i.e., >12%)[4,10] and a negative heat of mixing[4] are key factors favoring glass formation. For amorphous Al-alloys, glass formation is favored for multicomponent

[a)]Address all correspondence to this author.
e-mail address: lczhangimr@gmail.com and l.zhang@ifw-dresden.de
[b)]This author was an editor of this journal during the review and decision stage. For the *JMR* policy on review and publication of manuscripts authored by editors, please refer to http://www.mrs.org/jmr_policy.
DOI: 10.1557/JMR.2007.0156

compositions covering typical ranges of Al (80–92 at.%), rare-earth addition (3–20 at.%), and transition metal components (1–15 at.%).[7] Al-TM-RE metallic glasses have been reported to have tensile strengths of up to 1280 MPa,[11] which are at least two times higher than those found for conventional age-hardened Al-alloys.[1] However, due to their low glass-forming ability (GFA), the formation of Al-based metallic glasses is limited to the shape of thin ribbons (usually with a thickness <100 μm), which obviously restricts their practical use. To obtain bulk Al-based glassy products with thickness ⩾1 mm, many attempts have been made to improve the GFA[12–14] and to form[15–19] and/or subsequently consolidate glassy powders into bulk form using hot pressing or hot extrusion.[7,20,21] It is especially important for low GFA alloys (such as Al[15–21] and Ti-alloys[22–24]) to prepare glassy powders and subsequent consolidation into bulk samples with unlimited thickness and shapes utilizing the viscous flow behavior in the supercooled liquid region ΔT_x ($=T_x - T_g$, where T_g is the glass transition temperature and T_x is the onset crystallization temperature).[25]

In this work, the $Al_{85}Ni_9Nd_4Co_2$ alloy was chosen based on the results reported in Refs. 11, 26, and 27, which showed that Al-TM-RE alloys have high GFA when (i) the Al content is not very high (about 85–87 at.%)[11]; (ii) Ni is used as the TM (the addition of Ni is most effective for glass-formation), followed by Fe and Co additions[26]; (iii) Nd is used as the RE metal because, more than other RE metals, it facilitates the stability of the liquid structure over a larger compositional range[27]; and (iv) the chemical composition is optimized by adding a second TM to the basic Al-TM-RE composition.[11] Systematic investigations proved that this supplementary solute element (preferable a late TM with very low solid solubility in Al as, for example, Co) causes a dramatic increase in glass formation upon quenching by stabilizing the liquid structure due to a decrease of the atomic diffusivity of the solute element.[11] At the same time, it contributes to the improvement of the mechanical properties, i.e., microhardness, tensile strength, and stiffness.[26] The primary objectives of this work were to investigate the GFA of the $Al_{85}Ni_9Nd_4Co_2$ alloy and to elucidate the possibility to produce bulk amorphous and/or nanostructured Al-based alloys by combining melt-spinning (MS) and powder metallurgy techniques followed by warm consolidation. The thermal stability and the crystallization behavior of the glassy powders were also investigated. These data were used for subsequent powder consolidation experiments.

II. EXPERIMENTAL

Starting from elemental pieces having a purity higher than 99.9 wt%, a master alloy with a nominal composition of $Al_{85}Ni_9Nd_4Co_2$ was prepared by arc melting under a Ti-gettered argon atmosphere. Rapidly quenched ribbons of the alloy were synthesized in an argon atmosphere by induction melting the master alloy ingot and ejecting it onto a single copper roller with diameter of 0.20 m in a Bühler melt spinner. The tangential speed of the copper wheel was varied from 5 to 37 m/s. The as-spun ribbons were approximately 5–6 mm wide, 22–97 μm thick, and up to several meters long.

Milling experiments were carried out from different starting materials for comparison: (i) as-spun glassy ribbon and (ii) elemental powder mixture with a purity higher than 99.9 wt% and particle sizes smaller than 100 μm. Ribbon pieces cut from the as-spun glassy ribbon prepared at 21 m/s or the elemental powder mixture were loaded together with hardened steel balls in a hardened steel vial in an argon-filled glove box with less than 1 ppm O_2 and H_2O. A ball-to-powder weight ratio of 13:1 was used. The ball milling was performed with a Fritsch Pulverisette 5 planetary ball mill (Idar-Oberstein, Germany) with different rotational speeds of 180–300 rpm. For pulverizing the melt-spun ribbons, cryogenic milling was used to overcome the very high ductility of the ribbons and to retain their glassy structure. The application of a rather low integral milling intensity—that is, milling for short times with high impact energy or vice versa—was found to the most important in reducing the changes of the structure of the as-spun ribbons.[28] For the mechanical alloying, the milling was performed as a sequence of 15 min milling intervals interrupted by 15 min breaks to avoid a strong temperature rise and to suppress recovery processes in the low melting metal aluminum. The iron impurity due to wear debris from the milling tools and the oxygen content in the milled powders were examined using inductively coupled plasma emission spectroscopy and were found to be less than 0.5 at.% and 0.4 at.%, respectively.

The consolidation of the powders obtained from ribbons prepared at 21 m/s was performed at 513 K under high purity argon atmosphere by uniaxial hot pressing as well as by hot extrusion using a Weber hot-press facility under a pressure of about 700 MPa. Before compaction, the powders were first manually cold pressed under argon atmosphere to green bodies with a diameter of 10 mm. Prior to extrusion, green bodies were encapsulated into copper cans with 12 mm in outer diameter and 10 mm inner diameter. The billets were placed into the extrusion die with an extrusion rate of 5 and covered loosely with a 5 mm long copper plug to ensure that the extruded powder sample was completely ejected from the hot die after extrusion. The vacuum chamber containing the extrusion accessory was evacuated to about 2×10^{-3} Pa. The die was then heated at a heating rate of 40 K/min up to 513 K. When the extrusion temperature was reached (i.e., 513 K), the extrusion load was applied

and the billet was extruded with a speed of about 0.2 mm s^{-1}. The densities of the $Al_{85}Ni_9Nd_4Co_2$ master alloy and the consolidated samples were measured using the Archimedes method. The relative densities of the compacts (or volume fraction of the voids in the compacts) were estimated as the density ratio between the consolidated samples and the arc-melted master alloy, as described in Ref. 29.

Structural features were characterized by x-ray diffraction (XRD) using a Philips PW 1820 diffractometer (Eindhoven, The Netherlands) with monochromated Co K_α radiation ($\lambda = 0.178896$ nm) and by transmission electron microscopy (TEM) using a Philips CM 20 electron microscope. The thermal stability against crystallization was analyzed by differential scanning calorimetry (DSC) using a Perkin-Elmer DSC 7 calorimeter (Shelton, CT) under flowing purified argon with a heating rate of 40 K/min. A second heating run under identical conditions was used to determine the baseline. To confirm the reproducibility of the experimental results, at least three specimens were characterized for each case. Isothermal DSC measurements were carried out by annealing to different temperatures near the glass transition temperature with a heating rate of 40 K/min, then holding for 60 min. The melting behavior was examined using a Netzsch DSC 404 (Bavaria, Germany) with a heating rate of 20 K/min. Vickers microhardness (H_V) tests at room temperature were performed on a Shimadzu HMV-2000 hardness tester (Shimadzu Corp., Kyoto, Japan) with a static load of 0.2 N.

III. RESULTS AND DISCUSSION

A. Melt-spun ribbons

Figure 1 shows the XRD patterns of the as-spun $Al_{85}Ni_9Nd_4Co_2$ ribbons prepared at different wheel speeds. At all wheel speeds, the ribbons display the predominant characteristics of broad diffuse maxima, which indicates that a glassy state has been achieved during melt-spinning even at a slow wheel speed of 5 K/s. When the wheel speed is $\leqslant$12 m/s, the diffraction peaks of a face-centered-cubic α–Al phase are superimposed on the diffuse scattering maxima of the amorphous phase. In contrast, when the wheel speed is $\geqslant$13 m/s, no sharp diffraction peaks from α–Al phase are visible in the XRD patterns, only a diffuse first scattering maximum with a broad shoulder. The pattern with a halo peak and a broad shoulder is very typical for amorphous Al alloys with low concentration of RE.[7,30,31] The broad shoulder is attributed to the presence of some Al nanocrystals in the as-spun ribbons, as proved by TEM observation.[30,31] In addition, when the wheel speed increases, the positions of the diffuse maximum shift to smaller diffraction angles. The scattering vector, defined as $Q_p = 4\pi \sin\theta/\lambda$, of the broad diffuse maximum for the amorphous

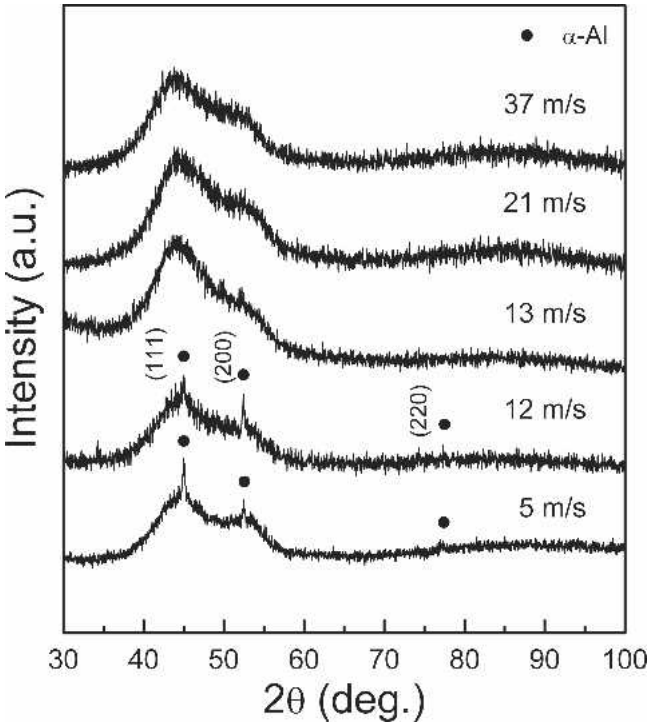

FIG. 1. XRD patterns of the melt-spun $Al_{85}Ni_9Nd_4Co_2$ ribbons prepared at different wheel speeds.

phase decreases from 26.56 nm^{-1} for the ribbon prepared at 5 m/s to 26.23 nm^{-1} for that prepared at 37 m/s. This implies that a higher Al content of the amorphous phase with increasing velocity, which leads to a change of the actual composition of the amorphous phase. It is noted that only the ribbons synthesized at wheel speeds $\geqslant$21 m/s are very ductile and can be bent 180° without fracture and the others prepared at <21 m/s are brittle.

Figure 2 shows the TEM bright-field micrographs and the corresponding selected area diffraction (SAED) patterns of the melt-spun $Al_{85}Ni_9Nd_4Co_2$ ribbons prepared at 5 and 21 m/s, respectively. For the ribbon obtained at 5 m/s, the TEM micrograph and the corresponding SAED pattern [Fig. 2(a)] reveal that the ribbon is composed of α–Al particles with a grain size of 20–30 nm and an amorphous phase. TEM observation of the ribbon prepared at 21 m/s [Fig. 2(b)] reveals that amorphous structure is the main feature of the ribbon. However, a very fine dispersion of α–Al nanocrystals with a grain size of 2–5 nm in the amorphous matrix is also visible. The diffuse halos together with the diffraction rings in the SAED pattern further demonstrate that the ribbon prepared at 21 m/s is in fact an α–Al nanocrystal/amorphous matrix composite. Thus, TEM observation confirms that the peak shoulder in the XRD patterns (Fig. 1) is related to the presence of Al nanocrystals, which is in agreement with the findings in Al–Y–Ni and Al–Ni–Ce metallic glassy ribbons.[30,31] EDX analysis indicates that the chemical composition of the amorphous

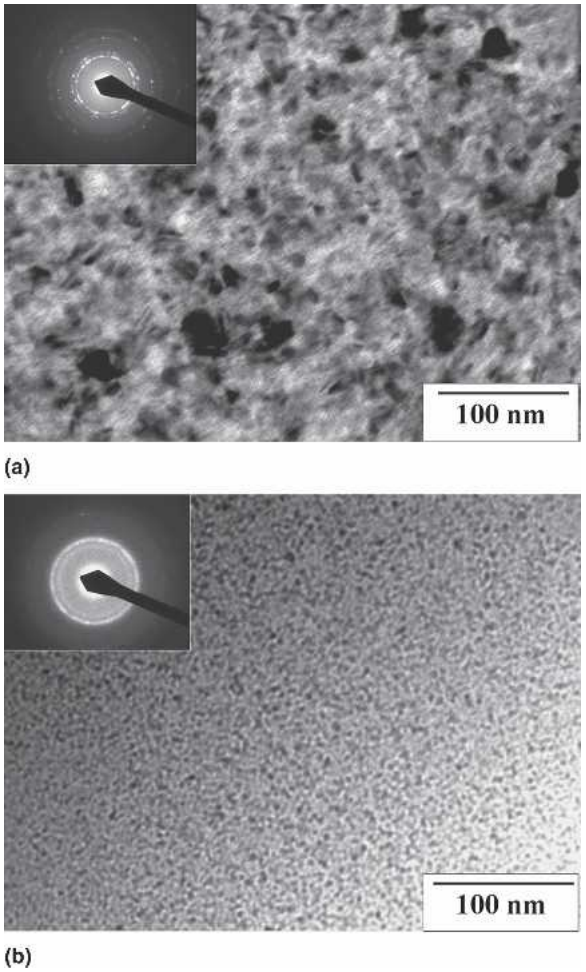

FIG. 2. TEM bright-field micrographs and the corresponding selected area diffraction patterns (inset) of the melt-spun $Al_{85}Ni_9Nd_4Co_2$ ribbons prepared at (a) 5 m/s and (b) 21 m/s.

matrix is approximately $Al_{83}Ni_{11.3}Nd_{3.3}Co_{2.4}$. The existence of nanocrystals in rapidly solidified products is common in Al-TM-RE marginal glass formation alloys.[8] This distribution of nanocrystals can catalyze crystallization upon reheating.[32]

Figure 3(a) displays the DSC scans in the mode of continuous heating at a heating rate of 40 K/min for the as-spun $Al_{85}Ni_9Nd_4Co_2$ ribbons prepared at different wheel speeds. In all cases, an endothermic signal associated with the glass transition and two main exothermic reactions caused by crystallization of the amorphous phase are evident, resulting in a supercooled liquid region before crystallization. Additionally, a weak exothermic peak in a range from around 450–520 K is observed, which may be due to structural relaxation and/or precipitation of nanoscale α–Al crystallites.[15] An enlarged view of a DSC trace near the glass transition showing the glass transition temperature (T_g) and the onset temperature (T_x) of the first crystallization event is given in Fig. 3(b). As the wheel speed increases [Fig. 3(a)], both the glass transition temperature and the crystallization temperature

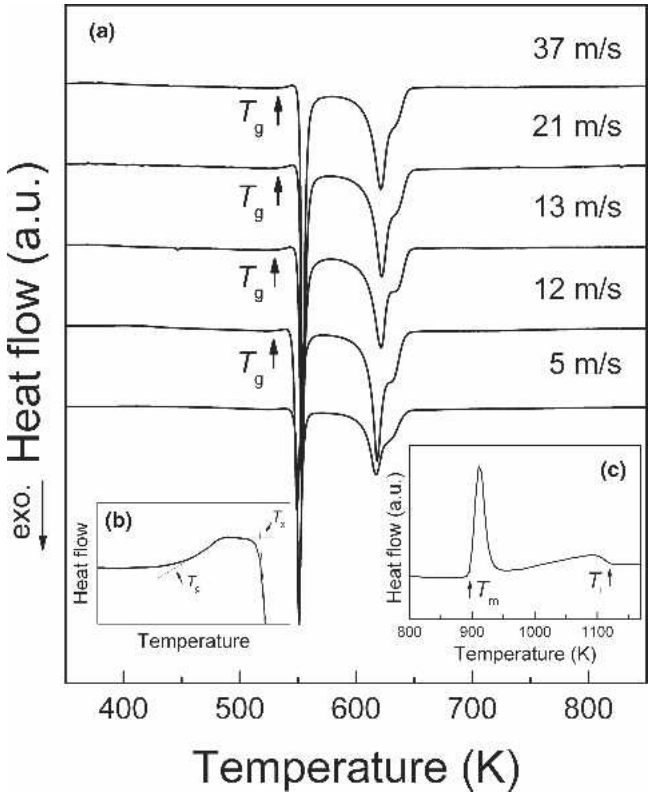

FIG. 3. (a) DSC scans of the melt-spun $Al_{85}Ni_9Nd_4Co_2$ ribbons prepared at different wheel speeds (heating rate 40 K/min), (b) an enlarged view of a DSC trace near the glass transition, and (c) melting behavior of the as-spun ribbon prepared at 21 m/s (heating rate 20 K/min).

shift to slightly higher temperatures, i.e., T_g and T_x increase from 528 and 548 K at 12 m/s to 533 and 553 K at 37 m/s. However, when the wheel speed is ⩾21 m/s, the glass transition temperature and the crystallization temperature stabilize at around 533 ± 1 and 553 ± 1 K, respectively, resulting in a supercooled liquid region of about 20 K. It has been reported that the thermal stability of amorphous Al alloys depends sensitively on composition.[9,26] As shown by the XRD patterns (Fig. 1) and TEM observation (Fig. 2), the ribbons prepared at the investigated velocities are amorphous-nanocrystalline composites, and the actual composition of the amorphous phase deviates from the nominal composition to a different extent with the changes of the wheel velocity. This can be proved from the EDX analysis results in TEM observation [Fig. 2(b)], which reveal that the actual composition of the amorphous phase deviates from the nominal composition. Therefore, the changes of the thermal stability of the ribbons prepared at different wheel velocities are attributed to the difference in the actual composition of the amorphous phase.

To examine the melting behavior of the $Al_{85}Ni_9Nd_4Co_2$ alloy, the ribbon obtained at 21 m/s was heated from room temperature to 1400 K with a heating rate of 20 K/min. The glass transition temperature and the onset

temperature of crystallization at this heating rate are 528 and 541 K, respectively. The melting behavior is illustrated in Fig. 3(c). It is characterized by a typical sharp endothermic event due to eutectic melting at T_m = 896 K and an extended tail of final melting with a liquidus temperature T_l = 1120 K. The fact that the liquidus temperature of the $Al_{85}Ni_9Nd_4Co_2$ alloy is much higher than the melting temperature of the main component Al ($T_{m,Al}$ = 933 K) indicates that the alloy is in fact far away from a eutectic composition, as is typical for Al-based metallic glasses.[7,9] Usually, "conventional" metallic glasses (such as Fe-, Zr-, and Cu-based, etc.) locate at or are close to a deep eutectic region, where the degree of supercooling required to form a glassy state is reduced and the liquid structure is stable at a temperature significantly lower than that of the glasses' main component.[33] That is, glass formation is favored in alloys with a high reduced glass transition temperature T_{rg} ($=T_g/T_l$)[33] and/or with a high γ [$=T_x/(T_g + T_l)$] value.[34] The $Al_{85}Ni_9Nd_4Co_2$ metallic glass has a T_{rg} value of 0.47 (comparable with that of Al–Ni–Fe–Gd glasses $T_{rg} \sim 0.44$[11]) and a γ value of 0.328. In general, these values of Al-based alloys are much lower than those of easy glass formers where a cooling rate as low as 100–1000 K/s is sufficient to produce the glassy state (i.e., $T_{rg} \sim 0.69$ and $\gamma \sim 0.464$ for $Pd_{40}Cu_{30}Ni_{10}P_{20}$; $T_{rg} \sim 0.63$ and $\gamma \sim 0.415$ for $Zr_{41.2}Ti_{13.8}Cu_{12.5}Ni_{10}Be_{22.5}$[34]).

From the above-mentioned XRD and DSC results, the $Al_{85}Ni_9Nd_4Co_2$ metallic glasses obtained at ⩾21 m/s are ductile, consist of a nanocomposite-type microstructure (consisting of an amorphous phase and α–Al nanocrystals), and have a distinct supercooled liquid region. Therefore, the $Al_{85}Ni_9Nd_4Co_2$ metallic glasses prepared at 21 m/s were used for further detailed investigations of their crystallization behavior to synthesize bulk Al nanostructured/glassy samples.

The isothermal DSC curves recorded at different annealing temperatures (T_a) close to T_g upon annealing the $Al_{85}Ni_9Nd_4Co_2$ metallic glass for 20 min are displayed in Fig. 4. When isothermal annealing at 513 K, only a monotonically decreasing signal rather than an exothermic peak is observed in the isothermal DSC curve, indicating a long incubation period (τ) of at least 20 min for crystallization at 513 K. XRD analysis [Fig. 5(b)] indicates that α–Al solid solution is precipitated from the amorphous phase after annealing at this temperature for 1 h. As seen from Fig. 4, for $T_a \geqslant 520$ K, all the isothermal DSC curves exhibit a monotonically decreasing signal with exothermic peaks associated with a nucleation and growth process[35] after a certain incubation period, suggesting that crystallization proceeds both by growth of pre-existing α–Al nanocrystals, followed by the nucleation and growth of crystallization products.[36] The incubation time as well as the time required for

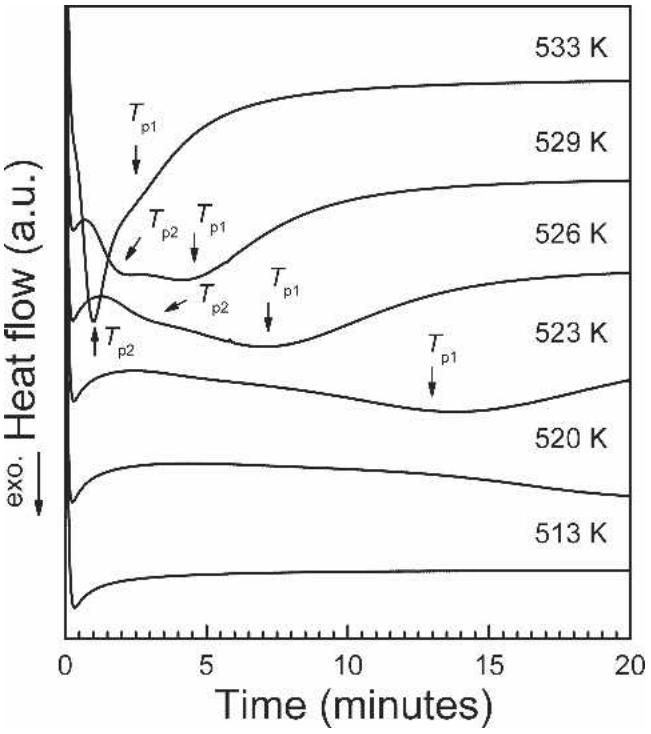

FIG. 4. Isothermal DSC curves recorded at different temperatures for the $Al_{85}Ni_9Nd_4Co_2$ ribbon prepared at 21 m/s.

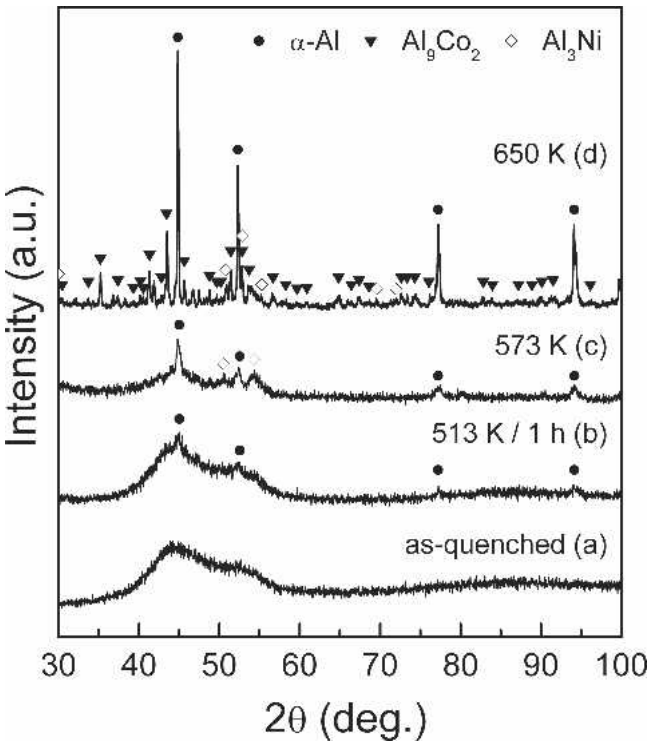

FIG. 5. XRD patterns measured at room temperature for the $Al_{85}Ni_9Nd_4Co_2$ ribbon prepared at 21 m/s: (a) as-spun ribbon, (b) after isothermal annealing at 513 K for 1 h, (c) after the first crystallization event at 573 K, and (d) after the second crystallization event at 650 K obtained for the samples scanned in the DSC at a heating rate of 40 K/min.

complete crystallization becomes shorter with annealing at higher temperatures, i.e., the incubation time decrease from around 6 min at 520 K to less than 1 min at 529 K. This can be ascribed to the higher atomic mobility at higher temperatures, which can establish the concentration fluctuations necessary for large-scale crystallization to set in.[35] It is noted that only one exothermic peak (T_{p1}) related to the crystallization event in the isochronal DSC curves shown in Fig. 3(a) is visible when $T_a \leqslant 523$ K. In contrast, another exothermic shoulder peak (T_{p2}) together with the former peak is also recorded when T_a is 526 K. Furthermore, T_{p2} shifts quickly to a shorter time as T_a increases. A similar phenomenon was also reported for the Ti-based amorphous alloys.[23] However, the reason for the exothermic peak split is not clear yet.

To identify the structural changes related to the two main crystallization events in the constant-rate heating DSC scans [Fig. 3(a)], the glassy ribbons were continuously heated in the DSC to the end temperatures of the two exothermic events (573 and 650 K, respectively) at a heating rate of 40 K/min, and then cooled down to room temperature at 100 K/min for subsequent XRD measurements. The XRD patterns are shown in Fig. 5. The formation of predominant α–Al solid solution and a small-volume fraction of Al_3Ni intermetallics are observed after continuously heating to the end temperature of the primary crystallization event (573 K) [Fig. 5(c)]. This crystallization behavior is not common for Al-TM-RE marginal glass-forming compositions with high Al-content,[37,38] which primarily crystallize into α–Al solid solution. However, compared with the crystallization product after isothermal annealing at 513 K for 1 h [Fig. 5(b)], it is still suitable for synthesizing high-strength nanostructured Al-based alloys by controlled crystallization.[39] In the second stage of crystallization [Fig. 5(d)], the residual amorphous phase further crystallizes, leading to the presence of α–Al phase, Al_9Co_2, and Al_3Ni compounds in the final crystallized products.

B. Ball-milled powders

Figure 6 compares the XRD patterns of as-milled $Al_{85}Ni_9Nd_4Co_2$ powders obtained from different starting materials with that of the as-spun glassy ribbons prepared at 21 m/s. When the as-spun glassy ribbon is milled for 9 h [Fig. 6(b)], a similar glassy/nanostructured structure to the initial ribbon [Fig. 6(a)] is obtained for the as-milled powder. The peak position of the diffuse diffraction maximum of the as-milled powder shifts to smaller angles than that of the initial ribbon does. The scattering vector Q_p of the broad diffuse maximum for the amorphous phase decreases from 26.42 nm^{-1} for the ribbon to 26.35 nm^{-1} for the powder. This can be ascribed to the chemical composition change of the amorphous phase and/or the increase of the free volume content during ball milling. In addition, it has been reported that nanocrystallization occurs upon milling.[40–43] In contrast, when the elemental powder mixture is milled for 140 h [Fig. 6(c)], only α–Al solid solution and Al_9Co_2 phase (no amorphous phase) dominate in the final product. Similar results were also reported for other Al-based alloys prepared by mechanical alloying.[18] The lattice parameter of α–Al solid solution is estimated by a Nelson–Riley extrapolation[44] to be $a = 0.406$ nm, which is about 1.2% smaller than that of the pure α–Al phase ($a_0 = 0.410$ nm), possibly resulting from the solid solution of Ni and Co with relatively smaller atomic size. Even after prolonged milling for up to 400 h, the milling process does not lead to a "crystal-to-glass" transition due to the severe sticking of Al to the milling tools, which causes a composition deviation from the desired composition to a significantly lower Al content (down to about 70 at.% Al) and, in turn, higher Ni, Nd, and Co contents.

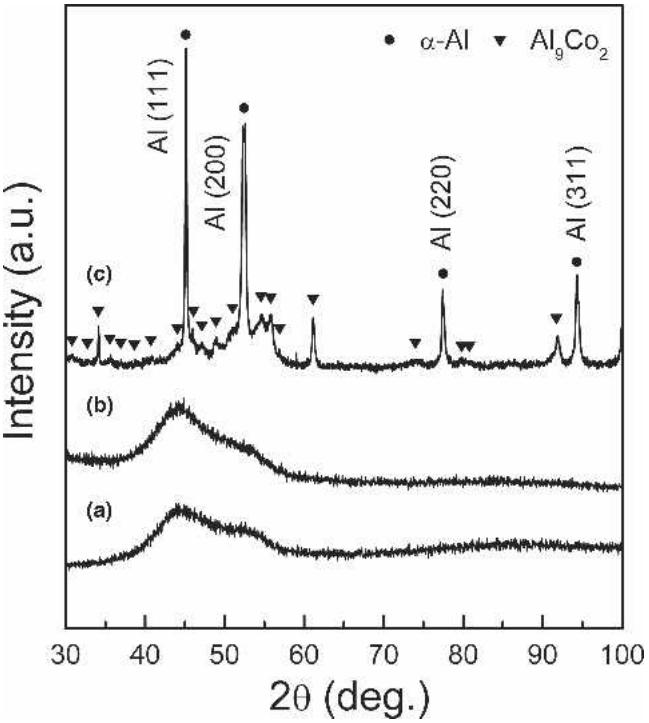

FIG. 6. XRD patterns of $Al_{85}Ni_9Nd_4Co_2$ samples in different states: (a) as-spun glassy ribbon prepared at 21 m/s, (b) as-milled powder prepared by milling the as-spun ribbon (milling parameters: 200 rpm, 9 h), and (c) as-milled powder obtained by mechanical alloying of the elemental powders mixture (180 rpm, 140 h).

Figure 7 compares the DSC curves for the as-spun $Al_{85}Ni_9Nd_4Co_2$ ribbon and the powders obtained from the ribbon after milling for 9 h. Both amorphous phases exhibit very similar thermal stability and crystallization behavior: a significant glass transition and a two-step crystallization process (although the split of the second exothermic peak is more apparent for the as-milled powders). However, for the milled powders, the glass transition temperature (T_g) as well as the onset (T_x) and peak temperatures (T_p) of the two crystallization events

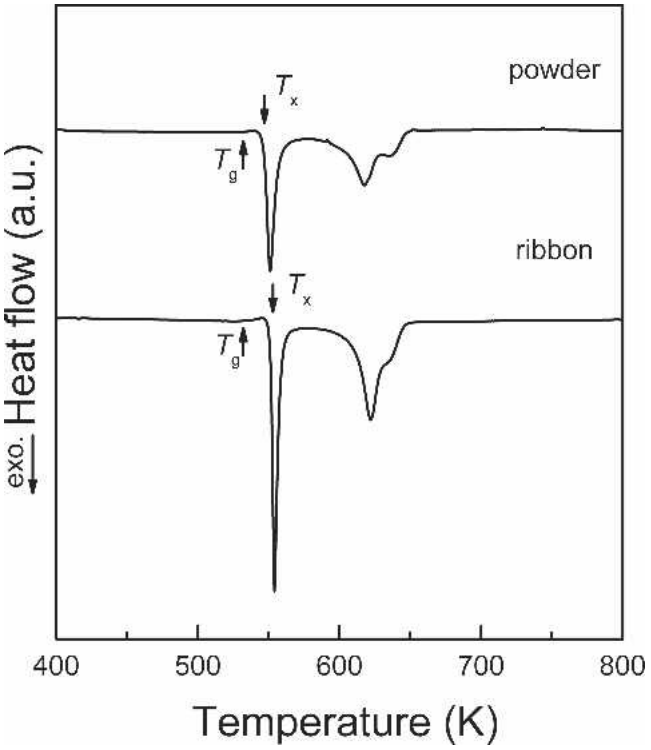

FIG 7. DSC scans of $Al_{85}Ni_9Nd_4Co_2$ samples in different states: (a) as-spun glassy ribbon (21 m/s) and (b) as-milled powder (200 rpm, 9 h) prepared from the ribbon.

slightly shift to lower temperatures, i.e., T_g, T_x, T_{p1}, and T_{p2} decrease from 533, 553, 554, and 622 K for ribbon to 532, 547, 551, and 618 K, respectively. The changes of thermal stability presumably result from a slight composition deviation from that of the initial ribbons after 9 h of milling. This can be proved from the heat release (ΔH_x) of the two crystallization events. The thermal properties including T_g, T_x, T_p, ΔT_x, ΔH_x evaluated from the DSC curves of both samples are summarized in Table I. The heat release of the powders (2.67 kJ/mol) is much smaller than that of the ribbons (3.53 kJ/mol). The decrease of the heat release indicates that partial crystallization (such as α–Al solid solution) occurs during the milling, resulting in a composition deviation of the glassy phase in the milled powders from that of the initial ribbons.[7] This may result from the nanocrystallization upon milling.[40–43] The milling induced crystallization is found to be very sensitive to the chemical composition of the amorphous alloys.[45–47] It is assumed that the volume fraction of the crystalline phase formed during the crystallization process associated with the DSC peak, or the volume fraction of the remaining metallic glass phase, can be estimated from the corresponding enthalpy release assuming that the area under the DSC peak is proportional to the volume fraction of crystals or residual amorphous phase, respectively.[48,49] Therefore, the volume fraction of the residual amorphous phase in the powder can be evaluated to be 76%. Thus, the composition of the amorphous phase is estimated to be approximately $Al_{80.2}Ni_{11.9}Nd_{5.3}Co_{2.6}$, supposing that only pure α–Al phase crystallizes and/or sticks to the milling media during the ball milling. Finally, the composition deviation leads to the shift of thermal stability of the powders.

To prepare bulk glassy or nanostructured samples by consolidation of the milled powders, it is necessary to correctly estimate the consolidation parameters (such as temperature and time) for avoiding or controlling the crystallization process. Thus, isothermal annealing at different temperatures was performed for the milled powders. Figure 8 displays the isothermal DSC curves of the powder milled for 9 h. When annealing at 513 K, only a monotonically decreasing signal is observed, indicating $\tau \geqslant 60$ min for crystallization at this temperature. In contrast, when $T_a \geqslant 520$ K, the incubation time decreases significantly with a slight increase in temperature when the annealing temperature changes by only 10 K (513–523 K), i.e., τ decreases from about 22 min at 516 K sharply to 2 min at 523 K, which will render the powder consolidation quite complicated and difficult for control. In addition, the incubation time at the temperature over 530 K is extrapolated to be less than 30 s following the above trend. Therefore, the incubation time at temperatures higher than 523 K ($\tau \leqslant 2$ min) is too short to be feasible for subsequent powder consolidation, which indicates that the suitable consolidation temperatures should be well below T_g. It is noted that there is a long time for the monotonically decreasing signal before the nucleation and growth process in all the isothermal DSC curves for both ribbons and powders, which is due to the grain growth of pre-existing α–Al nanocrytals. Comparing the time for the monotonically decreasing signal at a close temperature (i.e., 523 K), it is easy to find that the time for the powder (about 2 min) is shorter than that for the ribbon (about 6 min). This may result from the higher volume fraction of pre-existing α–Al nanocrystals in the

TABLE I. Glass transition temperature (T_g), onset (T_x) and peak (T_p) temperatures of crystallization, width of the supercooled liquid region (ΔT_x), and total heat release of crystallization (ΔH_x) obtained from the DSC measurements (heating rate of 40 K/min) for the $Al_{85}Ni_9Nd_4Co_2$ alloy processed by melt spinning and subsequent ball milling.

Samples	T_g (K)	T_{x1} (K)	T_{x2} (K)	T_{p1} (K)	T_{p2} (K)	ΔT_x (K)	ΔH_x (kJ/mol)
Melt-spun ribbon	533 ± 1	553 ± 1	611 ± 1	554 ± 1	622 ± 1	20 ± 1	3.53 ± 0.09
Ball-milled powder	532 ± 1	547 ± 1	603 ± 1	551 ± 1	618 ± 1	15 ± 1	2.67 ± 0.11

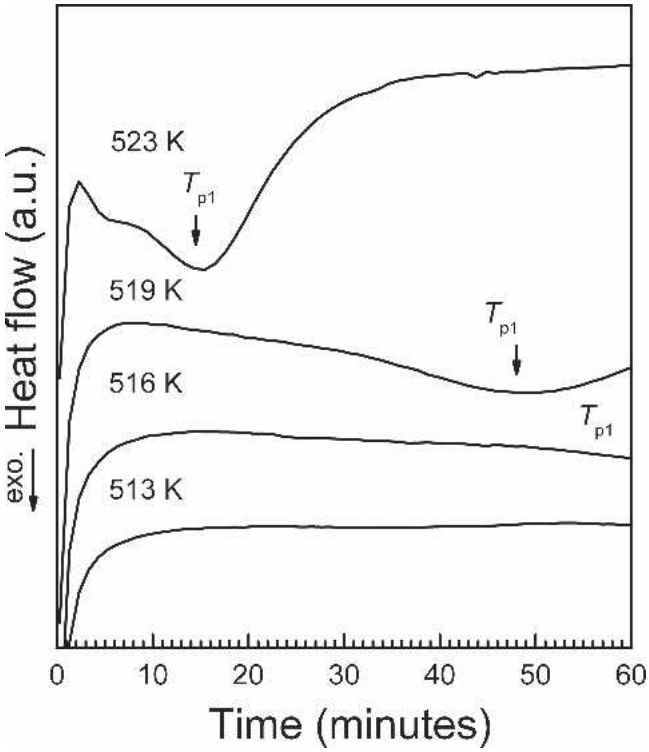

FIG 8. Isothermal DSC curves at different temperatures for the as-milled powder obtained by ball milling starting from the $Al_{85}Ni_9Nd_4Co_2$ ribbon (21 m/s).

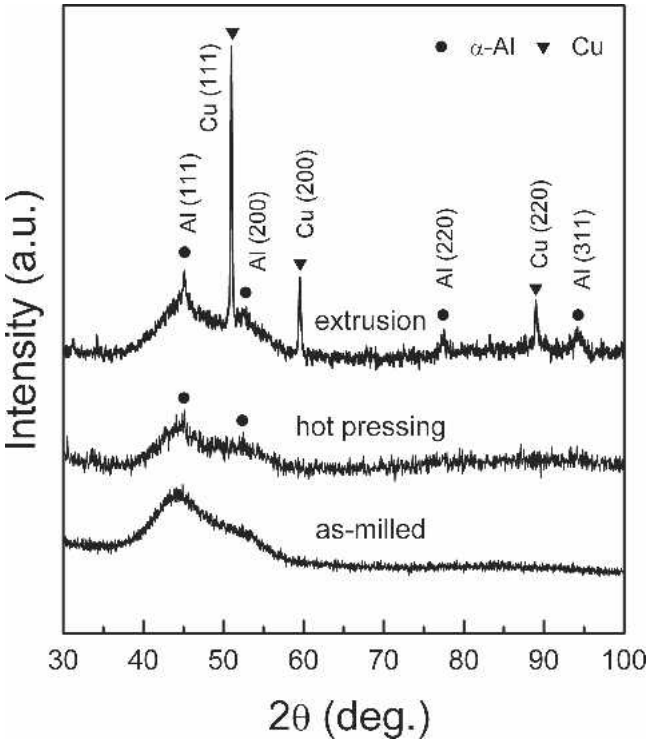

FIG. 9. XRD patterns of (a) as-milled powder and bulk samples after consolidation via (b) uniaxial hot pressing and (c) extrusion for the $Al_{85}Ni_9Nd_4Co_2$ alloy. (The Cu phase peaks stem from the Cu can used for encapsulation of the samples).

powder than in the ribbon, which act as heterogeneous nucleation sites and quickly saturate during isothermal annealing.[50]

C. Consolidation of the glassy powders

The isothermal DSC results were used for subsequent consolidation experiments to produce bulk glassy/nanostructured Al-based samples. Because at lower temperatures the deformation necessary for the material flow and, hence, for successful consolidation, is essentially hindered, the temperature of 513 K has been chosen as a compromise due to a long incubation time of about 60 min at this temperature. In this work, the two methods of uniaxial hot pressing and hot extrusion were attempted to consolidate the as-milled glassy powders obtained from the as-spun ribbons.

Figure 9 compares the XRD patterns for the bulk samples consolidated by uniaxial hot pressing and hot extrusion and the as-milled powder. For the hot-pressed sample, the broad diffuse maximum and a shoulder indicate that the compact has a structure quite similar to the milled powders and the initial ribbon (Fig. 6). However, there is about 6% volume fraction of voids in the hot-pressed compact.

In contrast, the extruded sample is a composite with nanostructured α–Al solid solution embedded in an amorphous matrix (the Cu phase peaks stem from the Cu can used for encapsulation of the samples). This kind of amorphous-nanocrystalline composite may have excellent mechanical properties combining high strength and high ductility.[51] At the same time, the extruded compact has higher density due to smaller residual porosity (<2%) in the sample compared with the hot-pressed specimens (~6%). Although the extrusion temperature (513 K) is low enough to avoid the time-dependent precipitation of α–Al as the first crystallization product (Fig. 8), about 24% volume fraction of nanostructured α–Al solid solution precipitates during extrusion. It has been reported that deformation induces nanocrystal formation in shear bands of Al-TM-RE metallic glass ribbon during bending[47] and nanocrystallization occurs during nanoindentation of Zr-based BMGs at room temperature.[52] The nanocrystallization at temperatures far below T_x is due to the rapid atomic diffusion ability enhancement during deformation.[47,52] It is clear that the initial reaction during the milling proceeds via nucleation and growth of the crystallized phase and therefore triggers a continuation of the reaction during the subsequent hot extrusion procedure.[28] One reason that may account for the precipitation of the α–Al phase even during the milling of as-spun ribbons is that the strong supersaturation of the rapidly quenched microstructure is highly sensitive to any further mechanical treatment.[28] Another important contribution to the occurrence of crystallization could come

from the work-induced heat generation during extrusion, which could cause a temperature rise in the billets.[53] The temperature rise in the billet can be estimated according to the semi-empirical relation[53]:

$$\Delta T = 1.1 \times 10^4 \cdot V_e^{0.64} \cdot P_e/(\rho \cdot C_p) \quad , \qquad (1)$$

where V_e is the ram speed, P_e the pressure during extrusion, ρ the bulk density of the alloy, and C_p its specific heat. The ram speed is 0.2 mm s^{-1}, and the extrusion pressure is about 0.7 GPa in our experiments. With a density for the nominal alloy of 3.50 g cm^{-3} and a specific heat of 24.64 J mol^{-1} K^{-1}, Eq. (1) gives a potential temperature rise of about 18 K. Adding this temperature to the nominal extrusion temperature of 513 K, the actual temperature that the sample experienced upon extrusion is about 531 K. However, as described before, the incubation time at 531 is very short ($\tau \leqslant 30$ s) to avoid the precipitation of α–Al. A similar phenomenon has also been reported in the case of Al–Mn–Ce extruded powders.[28] On the other hand, as seen from Fig. 5(b), long annealing time at 513 K leads to the precipitation of the α–Al phase from the amorphous phase. Therefore, it is much easier to precipitate the α–Al phase when the extrusion is done at higher temperature.

It is improper to test compressive mechanical properties due to the presence of up to about 6% voids in the compacts. Nevertheless, the mechanical properties evaluated by microhardness measurements are promising. Vickers microhardness tests give values of about 382 H_v for the as-spun ribbon prepared at 21 m/s, 380 H_v for the hot-pressed sample, and 350 H_v for the extruded sample. These values are much higher than those (100–190 H_v) of conventional high-strength crystalline Al-based alloys[1] and are comparable with those (340 H_v) reported for melt-spun amorphous $Al_{85}Ni_5Y_8Co_2$.[26] A rough estimate of potential ultimate strengths according to the empirical equation[54]:

$$\sigma_{UTS} = 3.7 \cdot H_v \quad , \qquad (2)$$

promises ultimate strengths of about 1310 MPa, which is similar to other Al-TM-RE glassy alloys.[7,26,28]

For full consolidation (without voids) of powders by extrusion and/or hot pressing, the interplay between consolidation pressure, incubation time, crystallization temperature, and viscous flow should be optimized. This seems to be rather difficult in the case of Al-based amorphous alloys because they generally have a rather narrow supercooled liquid region and an extremely high nucleation rate for crystallization.[39]

IV. SUMMARY

The glass/nanostructure formation in the $Al_{85}Ni_9Nd_4Co_2$ alloy was investigated by melt spinning and mechanical alloying. Amorphous/nanostructured ribbons were obtained by melt spinning at wheel surface velocities ranging from 5 to 37 m/s. The as-spun ribbon prepared at 21 m/s is ductile and exhibits a distinct glass transition as well as two crystallization events, resulting in a supercooled liquid region of about 20 K. T_{rg} and γ are estimated to be 0.47 and 0.328, respectively.

Mechanical alloying from the elemental powder mixture does not lead to a "crystal-to-glass" transition in the $Al_{85}Ni_9Nd_4Co_2$ alloy. The glass formation via mechanical alloying seems to be inaccessible due to the strong sticking of aluminum to the milling tools, which leads to pronounced composition deviations from the nominal composition. In contrast, an amorphous phase was retained after milling glassy ribbon for 9 h. The obtained powders exhibit a similar thermal stability to the as-spun ribbon.

The powders obtained from the ribbon were consolidated via uniaxial hot pressing and hot extrusion at 513 K, which was selected to be an optimum temperature according to the isothermal DSC measurements. Comparing the two consolidation methods, one can conclude that the extrusion essentially accelerates the time-dependent incubation time of the amorphous-to-crystalline phase transformation. Both types of bulk glassy/nanostructured composite have a high microhardness. However, the strong tendency for α–Al primary crystallization within the temperature range necessary for consolidation of the powders is the main barrier to the successful preparation of fully bulk glassy $Al_{85}Ni_9Nd_4Co_2$ alloys. Further investigations to consolidate bulk amorphous or composite samples are required by optimizing the consolidation parameters.

ACKNOWLEDGMENTS

The authors thank Dr. B. Rellinghaus for stimulating discussions and B. Bartusch, M. Frey, and C. Mickel for technical assistances. Two of the authors, L.C. Zhang and M. Calin, greatly appreciate the financial support from the Alexander von Humboldt Foundation. Funding from the European Union via the Research Training Network on "ductile bulk metallic glass composites" (Grant No. MRTN-CT-2003-504692) is also acknowledged.

REFERENCES

1. A.K. Vasudevan and R.D. Roherty: *Aluminium Alloys Contemporary Research and Application* (Academic Press, San Diego, CA, 1989).
2. M.J. Donachie, Jr.: *Titanium and Titanium Alloys* (American Society for Metals, Metals Park, OH, 1982).
3. W.L. Johnson: Bulk glass-forming metallic alloys: Science and technology. *MRS Bull.* **24,** 42 (1999).
4. A. Inoue: Stabilization of metallic supercooled liquid and bulk amorphous alloy. *Acta Mater.* **48,** 279 (2000).

5. Y. He, S.J. Poon, and G.J. Shiflet: Synthesis and properties of metallic glasses that contain aluminum. *Science* **241,** 1640 (1988).
6. A. Inoue, K. Ohtera, A.P. Tsai, and T. Masumoto: New amorphous alloys with good ductility in Al–Y–M and Al–La–M (M = Fe, Co, Ni or Cu) systems. *Jpn. J. Appl. Phys.* **27,** L280 (1988).
7. A. Inoue: Amorphous, nanoquasicrystalline and nanocrystalline alloys in Al-based systems. *Prog. Mater. Sci.* **43,** 365 (1998).
8. J.H. Perepezko, R.J. Hebert, and W.J. Tong: Amorphization and nanostructure synthesis in Al alloys. *Intermetallics* **10,** 1079 (2002).
9. Y. He, G. Dougherty, G.J. Shiflet, and S.J. Poon: Unique metallic glass formability and ultra-high tensile strength in A1–Ni–Fe–Gd alloys. *Acta Metall. Mater.* **41,** 337 (1993).
10. T. Egami and Y. Waseda: Atomic size effect on the formability of metallic glasses. *J. Non-Cryst. Solids* **64,** 113 (1984).
11. S.J. Poon, Y. He, G.J. Shiflet, and G. Dougherty: *Science and Technology of Rapid Solidification and Processing* (Kluwer Academic Publishers, New York, Boston, Dordrecht, London, Moscow, 1995), p. 43.
12. R.E. Hackenberg, M.C. Gao, L. Kaufman, and G.J. Shiflet: Thermodynamics and phase equilibria of the Al–Fe–Gd metallic glass-forming system. *Acta Mater.* **50,** 2245 (2002).
13. F.Q. Guo, S.J. Enouf, S.J. Poon, and G.J. Shiflet: Formation of ductile Al-based metallic glasses without rare-earth elements. *Philos. Mag. Lett.* **81,** 203 (2001).
14. Y.H. Kim, G.S. Choi, I.G. Kim, and A. Inoue: High-temperature mechanical properties and structural changes in amorphous Al–Ni–Fe–Nd alloys. *Mater. Trans., JIM* **37,** 1471 (1996).
15. I. Börner and J. Eckert: Phase formation and properties of mechanically alloyed amorphous $Al_{85}Y_8Ni_5Co_2$. *Scripta Mater.* **45,** 237 (2001).
16. P.P. Chattopadhyay, R.N.R. Gannabattula, S.K. Pabi, and I. Manna: Development of amorphous $Al_{65}Cu_{35-x}Ti_x$ alloys by mechanical alloying. *Scripta Mater.* **45,** 1191 (2001).
17. G.M. Dougherty, G.J. Shiflet, and S.J. Poon: Synthesis and microstructural evolution of A1–Ni–Fe–Gd metallic glass by mechanical alloying. *Acta Metall. Mater.* **42,** 2275 (1994).
18. T. Benameur and A. Inoue: Amorphization of aluminum base multicomponent systems by ball milling. *Mater. Trans., JIM* **36,** 240 (1995).
19. J. Eckert, L. Schultz, and K. Urban: Formation of quasicrystalline and amorphous phase in mechanically alloyed Al-based and Ti–Ni-based alloys. *Acta Metall. Mater.* **39,** 1497 (1991).
20. F. Schurack, J. Eckert, and L. Schultz: Synthesis and properties of mechanically alloyed and ball milled high strength amorphous or quasicrystalline Al-alloys. *J. Metast. Nanocryst. Mater.* **2,** 49 (1999).
21. A.P. Tsai, K. Aoki, A. Inoue, and T. Masumoto: Synthesis of stable quasicrystalline particle-dispersed Al base composite alloys. *J. Mater. Res.* **8,** 5 (1993).
22. L.C. Zhang, J. Xu, and E. Ma: Mechanically alloyed amorphous $Ti_{50}(Cu_{0.45}Ni_{0.55})_{44-x}$ $Al_xSi_4B_2$ alloys with supercooled liquid region. *J. Mater. Res.* **17,** 1743 (2002).
23. L.C. Zhang, Z.Q. Shen, and J. Xu: Mechanically milling-induced amorphization in Sn-containing Ti-based multicomponent alloy systems. *Mater. Sci. Eng., A* **394,** 204 (2005).
24. L.C. Zhang, Z.Q. Shen, and J. Xu: Thermal stability of mechanically alloyed boride/ $Ti_{50}Cu_{18}Ni_{22}Al_4Sn_6$ glassy alloy composites. *J. Non-Cryst. Solids* **351,** 2277 (2005).
25. Y. Kawamura, H. Kato, A. Inoue, and T. Masumoto: Fabrication of bulk amorphous alloys by powder consolidation. *Int. J. Powder Metall.* **33,** 50 (1997).
26. A. Inoue, N. Masumoto, and T. Masumoto: Al–Ni–Y–Co amorphous alloys with high mechanical strengths, wide supercooled liquid region and large glass-forming capacity. *Mater. Trans., JIM* **31,** 493 (1990).
27. A. Inoue, T. Ochiai, Y. Horio, and T. Masumoto: Formation and mechanical properties of amorphous A1–Ni–Nd alloys. *Mater. Sci. Eng., A* **179–180,** 649 (1994).
28. F. Schurack, J. Eckert, and L. Schultz: Al–Mn–Ce quasicrystalline composites: Phase formation and mechanical properties. *Philos. Mag.* **83,** 807 (2003).
29. L.C. Zhang, J. Xu, and E. Ma: Consolidation and properties of ball-milled $Ti_{50}Cu_{18}Ni_{22}Al_4Sn_6$ glassy alloy by equal channel angular extrusion. *Mater. Sci. Eng., A* **434,** 280 (2006).
30. S.J. Hong, P.J. Warren, and B.S. Chun: Nanocrystallization behaviour of Al–Y–Ni with Cu additions. *Mater. Sci. Eng., A* **304–306,** 362 (2001).
31. A.P. Tsai, T. Kamiyama, Y. Kawamura, A. Inoue, and T. Masumoto: Formation and precipitation mechanism of nanoscale Al particles in Al-Ni base amorphous alloys. *Acta Mater.* **45,** 1477 (1997).
32. J.H. Perepezko, R.J. Hebert, R.I. Wu, and G. Wilde: Atomistic simulations of the phase stability and elastic properties of nickel–zirconium alloys. *J. Non-Cryst. Solids* **317,** 52 (2003).
33. D. Turnbull and M.H. Cohen: Under what conditions can a glass be formed. *Contemp. Phys.* **5,** 473 (1969).
34. Z.P. Lu and C.T. Liu: A new glass-forming ability criterion for bulk metallic glasses. *Acta Mater.* **50,** 3501 (2002).
35. L.C. Chen and F. Spaepen: Analysis of calorimetric measurements of grain growth. *J. Appl. Phys.* **69,** 679 (1991).
36. A.L. Vasiliev, M. Aindow, M.J. Blackburn, and T.J. Watson: Phase formation during the devitrification of Al-rich melt-spun Al–8.5Ni–5.0Y–3.0(Co,Fe) alloys. *Scripta Mater.* **52,** 699 (2005).
37. P. Schumacher and A.L. Greer: Heterogeneously nucleated α-A1 in amorphous aluminium alloys. *Mater. Sci. Eng., A* **178,** 309 (1994).
38. D.R. Allen, J.C. Foley, and J.H. Perepezko: Nanocrystal development during primary crystallization of amorphous alloys. *Acta Mater.* **46,** 431 (1998).
39. M. Calin and U. Köster: Nanocrystallization of Al–Ni–Y and Al–Ni–Nd Metallic Glasses. *Mater. Sci. Forum* **269–272,** 749 (1998).
40. J. Eckert, L. Schultz, E. Hellstern, and K. Urban: Glass-forming range in mechanically alloyed Ni–Zr and the influence of the milling intensity. *J. Appl. Phys.* **64,** 3224 (1988).
41. J. Eckert, L. Schultz, and K. Urban: Amorphization reaction during mechanical alloying: Influence of the milling conditions. *J. Mater. Sci.* **26,** 441 (1991).
42. J. Eckert, L. Schultz, and K. Urban: Formation of quasicrystal by mechanical alloying. *Appl. Phys. Lett.* **55,** 117 (1989).
43. J. Eckert, L. Schultz, and K. Urban: Progress of quasicrystal formation during mechanical alloying in Al-Cu-Mn and the influence of the milling intensity. *Z. Metallkd.* **81,** 862 (1990).
44. L. Azaroff and M.J. Buerger: *The Powder Method in X-Ray Crystallography* (McGraw-Hill, New York, 1958), p. 238.
45. Y. He, G.J. Shiflet, and S.J. Poon: Ball milling-induced nanocrystal formation in aluminum-base metallic glasses. *Acta Mater.* **43,** 83 (1995).
46. W.H. Jiang and M. Atzmon: The effect of compression and tension on shear-band structure and nanocrystallization in amorphous $Al_{90}Fe_5Gd_5$: A high-resolution transmission-electron-microscopy study. *Acta Mater.* **51,** 4095 (2003).
47. H. Chen, Y. He, G.J. Shiflet, and S.J. Poon: Deformation-induced nanocrystal formation in shear bands of amorphous alloys. *Nature* **367,** 541 (1994).
48. L.C. Zhang, Z.Q. Shen, and J. Xu: Glass formation in a (Ti,Zr, Hf)–(Cu,Ni,Ag)–Al high-order alloy system by mechanical alloying. *J. Mater. Res.* **18,** 2141 (2003).
49. T. Gloriant, M. Gich, S. Suriñach, M.D. Baró, and A.L. Greer:

Evaluation of the volume fraction crystallised during devitrification of Al-based amorphous alloys. *Mater. Sci. Forum* **343–346,** 365 (2000).
50. E. Ma, C.V. Thompson, and L.A. Clevenger: Nucleation and growth during reaction in multiplayer Al/Ni films: The early stage of Al_3Ni formation. *J. Appl. Phys.* **69,** 2211 (1988).
51. A.L. Greer: Metallic glasses. *Science* **267,** 1947 (1995).
52. J.J. Kim, Y. Choi, S. Suresh, and A.S. Argon: Nanocrystallization during nanoindentation of a bulk amorphous metal alloy at room temperature. *Science* **295,** 654 (2002).
53. Y. Kawamura, A. Inoue, K. Sasamori, and T. Masumoto: Consolidation mechanism of aluminum-based amorphous alloy powders during warm extrusion. *Mater. Sci. Eng., A* **181–182,** 1174 (1994).
54. R. Hill: *The Mathematical Theory of Plasticity* (Oxford University Press, London, UK, 1967).